Supplementary Information (SI) for RSC Advances.

Supplementary Information (S.I.)

Influence of metal doping on the coke formation of a novel hierarchical HZSM-5 zeolite catalyst in the conversion of 1-propanol to fuel blendstock

1.0. Catalyst Characterisations

1.1. Phase identification of fresh catalysts

The pristine (fresh) hierarchical ZSM-5 zeolite exhibits a crystalline phase very similar to that of the standard ZSM-5 with JCPDS reference number 96-154-0268, as confirmed by its XRD pattern. Figure S1 shows the primary peaks of the catalysts, which can be seen at 2θ = 7–9° and 23–24° [1, 2]. The peaks observed at 7.97°, 8.88°, 14.8°, 23.1°, 23.3° and 24.0° correspond to the reflection planes (101), (200), (301), (501), (303) and (131) of the MFI structure of ZSM-5, which were retained after metal modification, indicating that the introduction of nickel species did not alter the framework [3]. XRD analysis revealed that the nickel species weighing 0.5 wt% may be too small to provide detectable signals and are undetectable [4, 5].

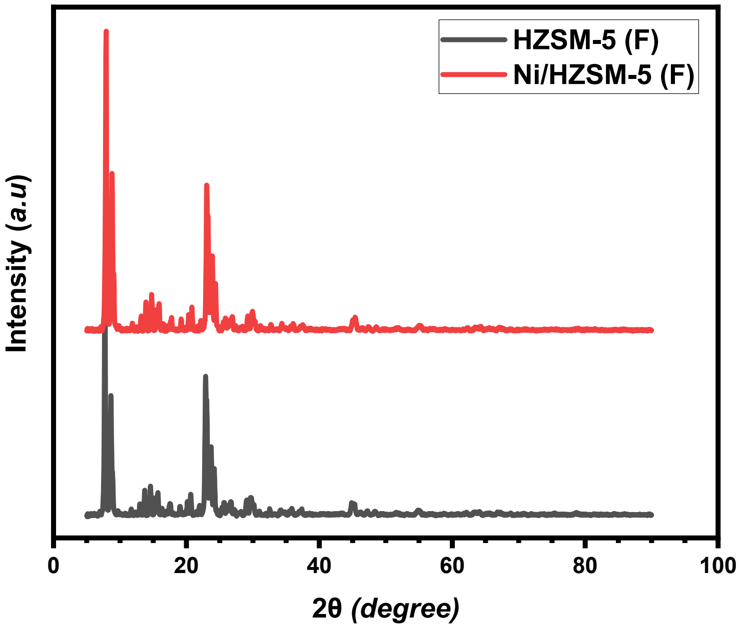

Figure S1. XRD patterns of fresh catalysts

1.2. Functional group identification for fresh catalysts

Figure S2 shows the absorption spectra of protonated ZSM-5 and Ni/HZSM-5 in the range from 4000 to 400 cm^{-1}. The absorption peaks in Figure S2 observed at the wavelengths 440, 543, 792, 1064, 1218, 1633, and 3646 cm^{-1} are consistent with the reference data of HZSM-5 presented in Table S1 [6, 7]. XRD and FTIR analyses of the crystal framework of the as-synthesised catalysts confirmed the successful synthesis conditions, and only the characteristic functional groups of the MFI zeolite could be detected, which is consistent with previous studies [6-8]. However, the small amount of metal species present might not be sufficient to generate distinct peaks for the corresponding nickel oxides, as shown by the lack of recognisable bands representing Ni oxides in the FTIR spectra.

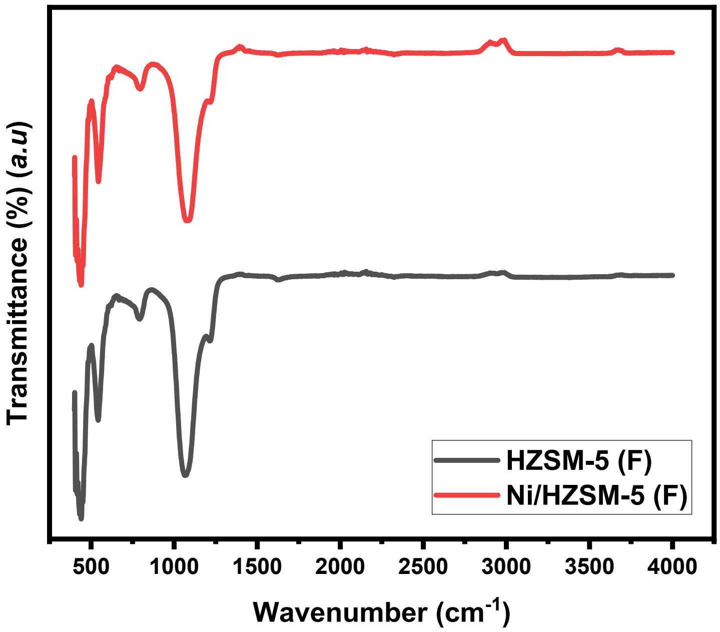

Figure S2. FTIR spectra of fresh catalysts

Table S1. FTIR wavenumbers and functional group representations for fresh catalysts

FTIR wavenumber (cm^{-1})	Functional group representation	Ref.
440	Tetrahedron units of SiO_4 and AlO_4	[7]
543	Pentasil zeolite structure's five-membered ring	[7]
792	Siloxane groups in a symmetrical manner	[9]
1064 and 1218	External and internal asymmetric stretching vibrations of the T-O band	[9]
1633	Deformational vibrations of water molecules	[9]
3646	Siloxane and hydroxyl groups	[10]

1.3. Catalyst morphology, particle size distribution and elemental composition

Microscopic images of the catalysts were taken with high-resolution SEM (Figure S3a). These micrographs allow the observation of particle size, shape and aggregation in both the pristine and metal-doped ZSM-5 crystals. At high magnification, prismatic crystals and nanoscale crystal aggregations in microspheres can be recognised. Estimating the primary particle size of ZSM-5 particles from SEM images alone is difficult as larger aggregates are formed consisting of several individual or interconnected zeolite particles. Therefore, PSD analysis was used to determine the particle size, and the results show that the distribution of particles for the catalysts ranges from 0.4 µm to over 100 µm (Figure S3b & c). In contrast to the unmodified catalyst, Ni-doped HZSM-5 shows a distribution with two different modes (bimodal), which can be attributed to several growth mechanisms, particle disintegration and the presence of large particles. The larger mode results from redispersion or fragmentation, while the smaller mode corresponds to the condensation of molecules [11, 12]. The particle sizes of the catalysts are 4.3 and 5.5 µm for HZSM-5 and Ni/HZSM-5, respectively. The composition of the nickel species in the doped catalyst was determined to be 0.52 by X-ray fluorescence (XRF).

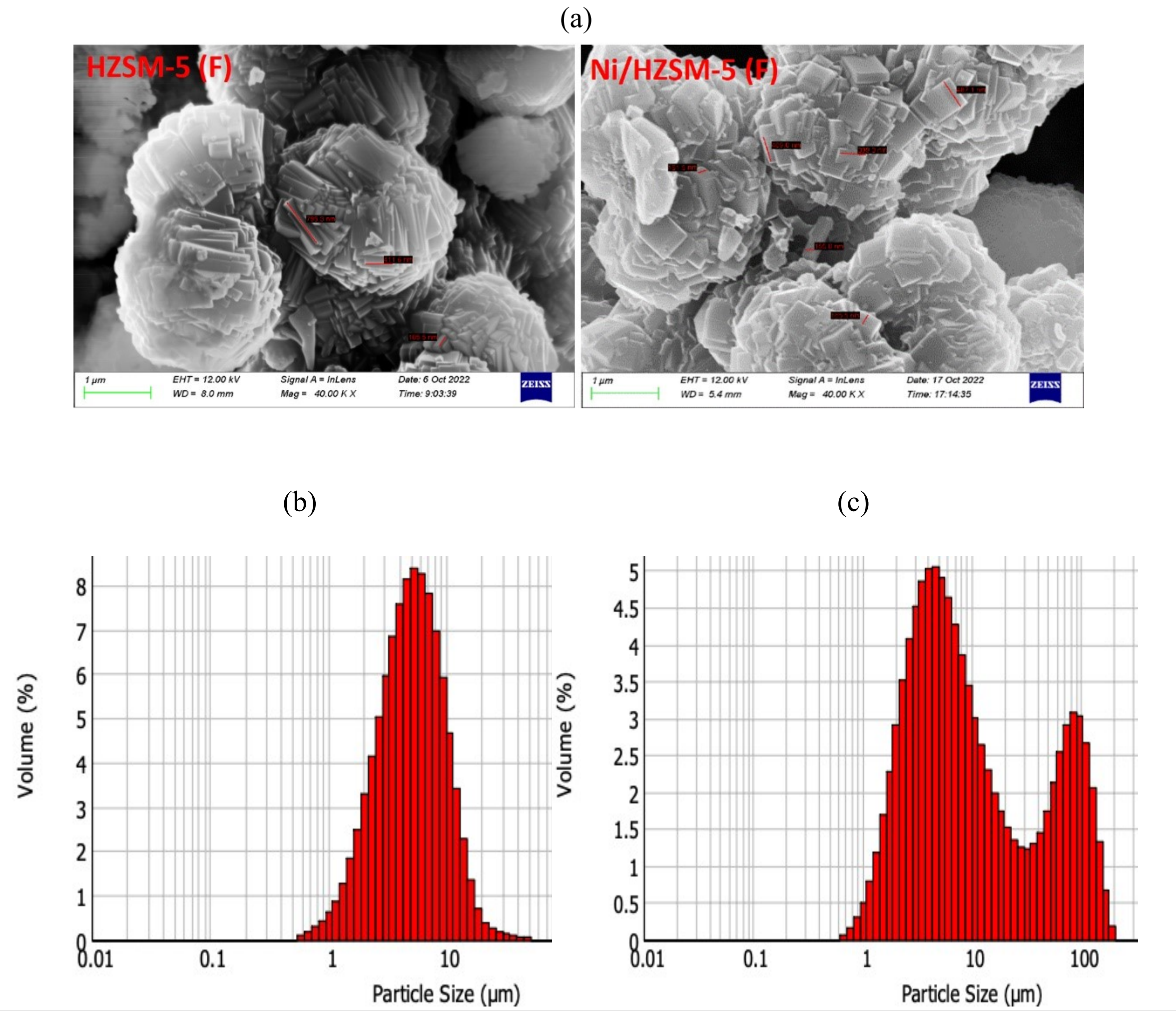

Figure S3(a) SEM micrographs fresh catalyst and PSD of (b) HZSM-5 and (c) Ni/HZSM-5 catalysts

1.4. Textural characteristics of fresh catalysts

N_2 adsorption-desorption analysis was used to determine the BET surface area of the fresh catalysts. From the data presented in Table S2, the BET surface area of the doped zeolites decreased from 397.48 $m^2\ g^{-1}$ for HZSM-5 to 381.36 $m^2\ g^{-1}$ for Ni/HZSM-5 catalysts. This showed that the surface of HZSM-5 was partially covered by nickel species, resulting in partial blockage of the zeolite channels. In addition, the pore volume of the catalysts reduced from 0.119 $cm^3\ g^{-1}$ for HZSM-5 to 0.077 $cm^3\ g^{-1}$ for Ni/HZSM-5 catalysts, while the pore diameter decreased slightly from 2.22 nm for ZSM-5 to 2.02 nm for Ni/HZSM-5. This supports the assumption that the Ni species coated the external surface of HZSM-5, resulting in significant clogging of the zeolite channels and hindering the entry of N_2 into the pores [13, 14]. The Barrett-Joyner-Halenda (BJH) method was used to analyse the low-temperature N_2 adsorption-desorption isotherm of fresh catalysts (Figure S4). All isotherms displayed a combination of type IV isotherms and H4 hysteresis loops [46, 47], occurring at a pressure, $P/P_0 > 0.4$. This behaviour indicates the presence of a hierarchically porous structure comprising mesopores and macropores. These loops are commonly associated with the capillary filling and condensation of nitrogen dioxide in uniform, slit-shaped intercrystalline mesopores formed by the cumulation of nano-sized zeolite crystals [15]. While there was a positive correlation between relative pressure and adsorbed volume, the amount of adsorption decreased with the introduction of nickel species. This decrease followed the order (adsorbed volume at STP), with HZSM-5 and Ni/HZSM-5 showing 109.94 and 104.61 $cm^3\ g^{-1}$, respectively, which correlates with the decrease in S_{BET} of the samples.

Table S2. Textural properties of fresh catalysts

Catalysts	S_{BET} ($m^2 g^{-1}$)	$V_{total (BJH)}$ ($cm^3 g^{-1}$)	$V_{meso (BJH)}$ ($cm^3 g^{-1}$)	$V_{macro (BJH)}$ ($cm^3 g^{-1}$)	Avg pore dia. (nm)	Volume @STP ($cm^3 g^{-1}$)	Metal loading (wt.%)
HZSM-5	397.48	0.7059	0.6775	0.0285	2.22	109.94	0.0
Ni/HZSM-5	381.36	0.5903	0.5820	0.0083	2.02	104.61	0.5

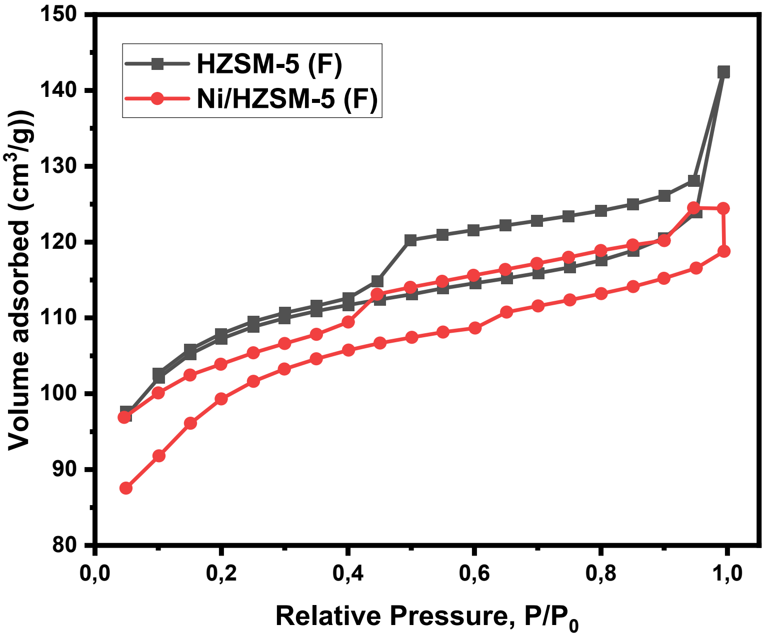

Figure S4. N_2 adsorption-desorption isotherm for fresh catalysts

1.5. Acidity results for as-synthesised (fresh) catalysts

The catalysts exhibited a three-part peak at several temperature intervals, corresponding to strong acidity (high temperature [HT] peak), moderate acidity (moderate temperature [MT] peak) and weak acidity (low temperature [LT] peak). This delineation was determined using NH_3-TPD analysis, which was used to evaluate the acidic characteristics of catalysts (Table S3). The weak acid sites (Lewis acid sites (LAS)), were attributed to Si-O-H and terminal -OH groups. In contrast, the strong acid sites (Bronsted acid sites (BAS)), were associated with bridging of -OH groups between Si/Al in the zeolite structure [16, 17]. The results show that the introduction of nickel species increases the LAS, with a decrease in the BAS. As a result of the integration of Ni into the HZSM-5, an increase of 11 % in the low-temperature bands was observed. Consequently, the amount of LAS for the Ni-doped catalyst increased from 950 µmol/g NH_3 for the HZSM-5 to 1060 µmol/g. This increase in weak acid sites could be due to the development of matching oxides (NiO), which act as LAS and thus increase the LAS. the moderately strong acid sites experienced a slight reduction of 7 %, leading to a decrease in the value of the Ni/HZSM-5 to 690 µmol/g. Conversely, a significant decrease of 42 % was recorded for the strong acidic sites for the Ni/HZSM-5. The B/L (strong/weak) acid ratio showed a higher value for the unmodified catalysts compared to the Ni-doped, which can be attributed to the higher BAS of the HZSM-5 catalyst. Total acidity increased by 3 %, attributed to an increase in LAS. Due to the presence of Ni ions within the zeolite structure, it is plausible that some acidic protons that accounts for the highly acidic sites undergo substitution, resulting in a decrease in their BAS [18].

Table S3. NH$_3$-TPD results for as-synthesised catalysts

Catalysts	**Peak Temp (°C)**			**Acidity concentration (μmol NH$_3$/g)**				
	L.T.	M.T.	H.T.	Weak	Moderate	Strong	Total acidity	Strong/Weak (B/L)
HZSM-5	198	419	686	950	740	24	1714	0.025
Ni/HSM-5	190	435	688	1060	690	14	1764	0.013

Reference

[1] Y. Peng *et al.*, "Fe-ZSM-5 supported palladium nanoparticles as an efficient catalyst for toluene abatement," *Catalysis Today,* vol. 332, pp. 195-200, 2019.

[2] I. M. S. Anekwe *et al.*, "Stability, deactivation and regeneration study of a newly developed HZSM-5 and Ni-doped HZSM-5 zeolite catalysts for ethanol-to-hydrocarbon conversion," *Catalysis Communications,* p. 106802, 2023.

[3] M. Yang *et al.*, "Conversion of lignin into light olefins and aromatics over Fe/ZSM-5 catalytic fast pyrolysis: Significance of Fe contents and temperature," *Journal of analytical and applied pyrolysis,* vol. 137, pp. 259-265, 2019.

[4] D. T. Sarve, S. K. Singh, and J. D. Ekhe, "Ethanol dehydration to diethyl ether over ZSM-5 and β-Zeolite supported NiW catalyst," *Inorganic Chemistry Communications,* vol. 139, p. 109397, 2022/05/01/ 2022, doi: https://doi.org/10.1016/j.inoche.2022.109397.

[5] G. Qi and R. T. Yang, "Ultra-active Fe/ZSM-5 catalyst for selective catalytic reduction of nitric oxide with ammonia," *Applied catalysis B: environmental,* vol. 60, no. 1-2, pp. 13-22, 2005.

[6] E. M. FLANIGEN, H. KHATAMI, and H. A. SZYMANSKI, "Infrared structural studies of zeolite frameworks," ACS Publications, 1971.

[7] H. Feng, C. Li, and H. Shan, "In-situ synthesis and catalytic activity of ZSM-5 zeolite," *Applied Clay Science,* vol. 42, no. 3, pp. 439-445, 2009/01/01/ 2009, doi: https://doi.org/10.1016/j.clay.2008.05.004.

[8] I. M. S. Anekwe, B. Oboirien, and Y. M. Isa, "Effects of Transition Metal Doping on the Properties and Catalytic Performance of ZSM-5 Zeolite Catalyst on Ethanol-to-hydrocarbons Conversion," *Fuel Communications,* p. 100101, 2023.

[9] N. Subramanian, J. Vijaya, S. Sivasanker, R. Chinnadurai, S. Thangaraju Murugan, and L. Kennedy, "Hierarchical ZSM-5 catalytic performance evaluated in the selective oxidation of styrene to benzaldehyde using TBHP," *Journal of Porous Materials,* vol. 23, 06/01 2016, doi: 10.1007/s10934-016-0129-8.

[10] V. P. S. Caldeira, A. G. D. Santos, S. B. C. Pergher, M. J. F. Costa, and A. S. Araujo, "USE OF A LOW-COST TEMPLATE-FREE ZSM-5 FOR ATMOSPHERIC PETROLEUM RESIDUE PYROLYSIS," *Química Nova,* vol. 39, 2016.

[11] J. Niu, P. Rasmussen, R. Magee, and G. Nilsson, "Spatial and temporal variability of incidental nanoparticles in indoor workplaces: Impact on the characterization of point source exposures," *Environmental science. Processes & impacts,* vol. 17, 11/20 2014, doi: 10.1039/c4em00478g.

[12] B. Li, X. Lin, Y. Luo, X. Yuan, and X. Wang, "Design of active and stable bimodal nickel catalysts for methane reforming with CO2," *Fuel Processing Technology,* vol. 176, pp. 153-166, 2018.

[13] A. López, I. De Marco, B. Caballero, A. Adrados, and M. Laresgoiti, "Deactivation and regeneration of ZSM-5 zeolite in catalytic pyrolysis of plastic wastes," *Waste management,* vol. 31, no. 8, pp. 1852-1858, 2011.

[14] Y. Li, D. Yellezuome, C. Li, and R. Liu, "Deactivation mechanism and regeneration effect of bi-metallic Fe-Ni/ZSM-5 catalyst during biomass catalytic pyrolysis," *Fuel,* vol. 312, p. 122924, 2022.

[15] A. Jawad and S. Ahmed, "Analysis and process evaluation of metal dopant (Zr, Cr)-promoted Ga-modified ZSM-5 for the oxidative dehydrogenation of propane in the presence and absence of CO 2," *RSC advances,* vol. 13, no. 16, pp. 11081-11095, 2023.

[16] B. Saini, A. P. Tathod, J. Diwakar, S. Arumugam, and N. Viswanadham, "Nickel nano-particles confined in ZSM-5 framework as an efficient catalyst for selective hydrodeoxygenation of lignin-derived monomers," *Biomass and Bioenergy,* vol. 157, p. 106350, 2022/02/01/ 2022, doi: https://doi.org/10.1016/j.biombioe.2022.106350.

[17] R. C. Deka, "Acidity in zeolites and their characterization by different spectroscopic methods," 1998.

[18] Z. Y. Zakaria, J. Linnekoski, and N. A. S. Amin, "Catalyst screening for conversion of glycerol to light olefins," *Chemical Engineering Journal,* Article vol. 207-208, pp. 803-813, 2012, doi: 10.1016/j.cej.2012.07.072.